

# Controlling the gap of fullerene microcrystals by applying pressure: the role of many-body effects

Murilo L. Tiago and Fernando A. Reboredo

*Oak Ridge National Laboratory, Oak Ridge, TN, 37831*

(Dated: November 3, 2018)

## Abstract

We studied theoretically the optical properties of  $C_{60}$  fullerene microcrystals as a function of hydrostatic pressure with first-principles many-body theories. Calculations of the electronic properties were done in the GW approximation. We computed electronic excited states in the crystal by diagonalizing the Bethe-Salpeter equation (BSE). Our results confirmed the existence of bound excitons in the crystal. Both the electronic gap and optical gap decrease continuously and non-linearly as pressure of up to 6 GPa is applied. As a result, the absorption spectrum shows strong redshift. We also obtained that “negative” pressure shows the opposite behavior: the gaps increase and the optical spectrum shifts toward the blue end of the spectrum. Negative pressure can be realized by adding cubane ( $C_8H_8$ ) or other molecules with similar size to the interstitials of the microcrystal. For the moderate lattice distortions studied here, we found that the optical properties of fullerene microcrystals with intercalated cubane are similar to the ones of an expanded undoped microcrystal. Based on these findings, we propose doped  $C_{60}$  as active element in piezo-optical devices.

PACS numbers: 1.48.-c, 2.50.-p, 71.35.Cc

## I. INTRODUCTION

Since its discovery,  $C_{60}$ <sup>1</sup> has been characterized as the most stable member in the series of fullerenes, which are pure-carbon molecules with the shape of spherical shells<sup>2</sup>.  $C_{60}$  can be produced economically and in abundance<sup>3</sup>. Its chemical bonds have strong  $sp^2$  character, making the shell very stiff and at the same time free of dangling bonds. Together with clathrates and other carbon-based materials, fullerenes are being actively investigated as building blocks for novel materials with unusual mechanical properties<sup>4,5</sup>. Fullerenes has remarkable properties, for example:  $C_{60}$  doped with alkali and alkali-earth atoms is superconductor<sup>6,7</sup>; it has been claimed that  $C_{60}$  can be heavily hydrogenated with up to 36 hydrogen atoms per molecule, making it a promising material for hydrogen storage<sup>8</sup>.

In pure form,  $C_{60}$  crystallizes in a molecular solid (fullerite), bound by weak forces between molecules. Its phase diagram is very rich, with a low-temperature face-centered cubic (FCC) phase, amorphous phases at intermediate temperature, and a diamond-like phase at high temperature. The FCC phase has rotational disorder and it is stable under pressure in excess of 15 GPa at room temperature<sup>9</sup>. Its energy gap is in the visible range, around 2 eV<sup>2,10</sup>. The softness and stability of fullerite could make it a good candidate for piezo-optical devices, where external pressure is applied reversibly and it modifies the optical response of the material. In addition, when fullerite is heavily doped with molecules of appropriate size, it behaves as if it is under “negative pressure”<sup>11</sup>. To that end, it is important to characterize the pressure dependence of the optical properties of this material. Extensive experimental work has been done on this direction<sup>10,12,13,14,15,16,17</sup>. A review of the literature can be found in Reference 9. Theoretical analyses are not so extensive, mostly concentrated on characterization at zero pressure<sup>18,19,20</sup>. In order to fill this vacuum, we present a systematic analysis of the optical properties of fullerite at pressures ranging from zero to 6 GPa. We also investigate the optical response of the crystal at “negative” pressure, which can be realized in laboratory, for instance, by doping fullerite with weakly interacting molecules such as cubane ( $C_8H_8$ ). Numerical accuracy is essential, which is why we use state-of-the-art theories, namely many-body Green’s function theories based on the GW-BSE approach.

This article is organized as follows: we outline the theoretical framework in section II. That section is followed by a discussion of results at zero pressure in section III, results at finite hydrostatic pressure in section IV and finally a description of the cubane-fullerene

compound, which resembles fullerite with “negative pressure”, in section V. Finally, we conclude with some perspectives of future applications and a summary.

## II. THEORY

The underlying electronic structure of fullerene is determined using density-functional theory (DFT)<sup>21</sup>. We use a plane-wave basis to solve the Kohn-Sham equations with cut-off in the kinetic energy of 50 Ry. Interactions involving valence electrons and core electrons are taken into account using norm-conserving pseudopotentials of the Troullier-Martins type<sup>21</sup>. We use the Perdew-Burke-Ernzerhof functional<sup>22</sup> (PBE) for exchange and correlation, based on the generalized-gradient approximation (GGA). It is well-known that DFT in the local-density approximation (LDA) or the PBE severely underestimates electronic gaps in general, making it unsuitable for detailed studies of optical properties of electronic systems. Accurate bandwidths and electronic energy gaps are calculated in a many-body framework within the GW approximation<sup>23</sup>. In that approximation, the electron self-energy is computed by summing up Feynman diagrams to lowest order in the screened Coulomb interaction. At lowest order, the self-energy becomes a product between the one-electron Green’s function  $G$  and the screened Coulomb interaction  $W$ , hence the name. We ignore vertex diagrams and we assume that Kohn-Sham eigenvalues and eigenvectors give a good approximation to the Green’s function. Formally, the self-energy in space-energy representation is written as

$$\Sigma(\mathbf{r}, \mathbf{r}'; E) = \frac{i}{2\pi} \int dE' e^{-i0^+ E'} G_0(\mathbf{r}, \mathbf{r}'; E - E') W_0(\mathbf{r}, \mathbf{r}'; E') \quad , \quad (1)$$

where  $G_0$  denotes the DFT-PBE Green’s function and  $W_0$  is the screened Coulomb interaction, related to the random phase approximation (RPA) dielectric function by:

$$W_0(\mathbf{r}, \mathbf{r}'; E) = \int d\mathbf{r}'' \epsilon^{-1}(\mathbf{r}, \mathbf{r}''; E) \frac{q_e^2}{|\mathbf{r}'' - \mathbf{r}'|} \quad . \quad (2)$$

In the present formulation, the dielectric function is expanded in a basis of plane waves with cut-off 9.5 Ry. Its energy dependence is described by a generalized plasmon pole model<sup>23</sup>. After the self-energy is computed, we diagonalize the quasi-particle Hamiltonian,  $H = H_{PBE} + \Sigma - V_{xc}$ <sup>23,24</sup>. Eigenvalues of that Hamiltonian provide the electronic band structure of the real material. This formulation is one of the simplest *ab initio* formulations of the GW approximation. Extensive applications of this formulation to a wide class

of carbon-based materials have shown it to predict electronic band gaps with an accuracy of 0.1 to 0.2 eV<sup>24,25</sup>. In the specific case of fullerite, the first calculation of electronic gap within the GW approximation was consistent with direct/inverse photoemission spectra<sup>18</sup>. Owing to the fact that hydrostatic pressure on fullerite microcrystals does not affect their electronic properties besides an increase in intermolecular interactions, we expect our theoretical methodology to be equally reliable in describing the pressure dependence of the electronic gap. Technical details about the theory can be found in review articles<sup>24,25</sup>.

The electronic band structure often does not give access to optical spectra because, after electron-hole pairs are excited, they interact and produce bound excitons, with energy lower than the electronic gap<sup>25,26</sup>. We describe the dynamics of excitons by diagonalizing the Bethe-Salpeter equation (BSE) for electrons and holes. The BSE is an equation for the two-particle Green's function. Written as an eigenvalue equation, its solution gives the energy of optical excitations in the material:

$$(E_c - E_v)A_{vc}^s + \sum_{v'c'} K_{v'c'}^{vc} A_{v'c'}^s = \Omega^s A_{vc}^s . \quad (3)$$

where  $\Omega^s$  is the excitation energy of optical modes, indexed by  $s$ , and  $A_{vc}^s$  are the corresponding eigenvectors.  $K_{v'c'}^{vc}$  is the electron-hole interaction kernel, written in the basis of pair transitions.

In the absence of electron-hole interactions ( $K = 0$ ), each excitation energy is simply the difference between quasi-particle energies of electrons ( $E_c$ ) and holes ( $E_v$ ). The kernel  $K$  adds two types of interactions: an electrostatic interaction mediated again by  $W_0$ ; and a repulsive exchange interaction between electron and hole, which is related to the fact that they can annihilate each other<sup>27</sup>. We follow the standard procedure to build and solve the BSE. We ignore the energy dependence of the interaction kernel and we assume the Tamm-Dancoff approximation<sup>27</sup> when computing  $K$ . Both approximations have been used extensively and they were shown to simplify considerably the numerical complexity, with little impact on numerical accuracy. This methodology has been presented in great detail elsewhere<sup>25,26,28</sup>.

Although numerically expensive, the GW-BSE theory has been remarkably successful in predicting electronic and optical properties of real materials without the need for phenomenological parameters<sup>24,25</sup>. All the approximations involved, such as the plasmon pole

model and the non-self-consistent assumption, are unambiguously defined. In addition, *sp*-bonded systems such as carbon-based nanostructures seem to be the ideal materials for this theory, owing to the fact that they have very weak correlation effects<sup>25,29,30</sup>.

### III. FULLERITE AT ZERO PRESSURE

The phase diagram of C<sub>60</sub> is extremely complex. At zero pressure and temperature, it crystallizes in a structure where the orientation of molecules is random but the molecules form a face-centered cubic (FCC) structure with lattice parameter around 14.2 Å<sup>9</sup>. At room temperature and under mechanical pressure of 8 GPa, the crystals were found to polymerize in several phases, with substantial distortion of the cage<sup>14,16</sup>. Since we are primarily concerned with hydrostatic pressure, we do not consider anisotropic pressure in this article. With increasing hydrostatic pressure, the lattice parameter decreases continuously according to Vinet equation of state<sup>13</sup>. The energy threshold of optical transmission also decreases<sup>15</sup>, following the reduction in lattice parameter. Other absorption edges are also known to redshift with applied pressure<sup>10</sup>.

In our calculations, we apply pressure indirectly by fixing the lattice parameter and using Vinet equation to map lattice parameter into hydrostatic pressure<sup>13</sup>:

$$p(a) = 3\kappa_0 \frac{1-x}{x^2} \exp \left[ \frac{3}{2}(\kappa'_0 - 1)(1-x) \right], \quad (4)$$

using a bulk modulus  $\kappa_0 = 18.1 \pm 1.8$  GPa and its pressure derivative  $\kappa'_0 = 5.7 \pm 0.6$ <sup>13</sup>. The parameter  $x$  is the ratio between lattice parameters,  $x = a/a_0$ . The lattice is built in the  $Pa\bar{3}$  (= *cP12*) structure, with one molecule per periodic cell.

Figure 1 shows the calculated electronic and optical gaps for several choices of lattice parameter. At zero pressure, we obtain an electronic gap of 2.1 eV, in full agreement with previous work and compatible with photoemission and inverse photoemission data<sup>18</sup>. Our DFT-PBE gap is 1.2 eV. The minimum gap is direct, around the crystallographic  $X$  point.

The C<sub>60</sub> molecule has icosahedral symmetry, belonging to the  $I_h$  point group<sup>31</sup>. Owing to its high symmetry, most molecular orbitals cluster in degenerate multiplets. The three highest occupied multiplets belong to symmetry representations denoted as  $H_u$ ,  $G_g$ , and  $H_g$  (ordered from highest energy to lowest energy), with degeneracies 5, 4 and 5 respectively. The lowest unoccupied multiplet in molecular C<sub>60</sub> has symmetry  $T_{1u}$ , followed by a  $T_{1g}$

multiplet, both with degeneracy 3.

In fullerite, each molecular multiplet originates a set of quasi-degenerate bands. The wavefunctions retain most of the shape of the molecular orbitals, so that they can still be labeled by symmetry representations of the molecular orbitals. The bandwidth of the  $H_u$  quintuplet, at the top of the valence bands, is 0.5 eV. The next multiplet is a  $T_{1u}$  triplet, with approximately the same bandwidth. Within the GW theory, these bandwidths are slightly larger than the ones calculated with DFT-PBE. There are two major differences between band structures predicted with GW and DFT-PBE: (1) widening of the electronic gap, and (2) small stretch of bands according to the expressions:

$$\begin{aligned}
 E_{GW}^{val.} &= E_{PBE}^{val.} \times 1.2 + 0.6 \text{ eV} \\
 E_{GW}^{cond.} &= E_{PBE}^{cond.} \times 1.2 + 1.25 \text{ eV} \quad , \quad (5)
 \end{aligned}$$

respectively for valence and conduction bands. In the equation above, the energies  $E_{GW}$  and  $E_{PBE}$  are given with respect to the DFT-PBE valence band maximum.

We determine the optical gap as the minimum excitation energy obtained after diagonalizing the BSE. This gap at equilibrium lattice constant is calculated to be 1.7 eV. The oscillator strength associated to this excitation is very weak, owing to a molecular selection rule that prevents optical absorption from the  $H_u$  to the  $T_{1u}$  multiplets. Significant absorption is found around 2.2 eV, corresponding to  $H_u$ - $T_{1g}$  transitions, as shown on Figure 3. The measured transmission edge is 1.9 eV<sup>15</sup>. This is compatible with our calculated results, considering the difficulties in determining the onset of absorption experimentally and the orientational disorder in the lattice, which is not included in our calculations. One of the earliest measurements of absorption spectra of crystalline C<sub>60</sub> identified peaks at 2.0 eV, 2.7 eV and 3.5 eV. Our calculations show peaks at 2.2 eV and 3.6 eV.

The inset of Figure 1 shows the maximum exciton binding energy, defined as the difference between electronic gap and optical gap. The binding energy is high: around 0.4 eV. As discussed above, it arises primarily from the Coulomb attraction between electrons and holes, which is large compared with other solids because of a weak dielectric screening. The first bound exciton has well-defined Frenkel character, which is compatible with the fact that its binding energy is close to the electron and hole bandwidths.

Figure 2 depicts the probability distribution of the electron given that the hole is fixed

on the surface of the central molecule. There are sharp maximums of probability on the central molecule, with more diffuse features in the neighbor molecules.

In order to quantify the exciton radius, we have computed the integrated electron-hole probability and listed it on the third column of Table I. For the first bound exciton, the probability of locating electron and hole on the same molecule is 62%. The probability of locating the electron on any of the nearest neighbors molecule relative to the hole site is substantially smaller (30%), decreasing then to 2% if the electron is on any second nearest neighbor. Excitons with lower binding energy (and higher excitation energy) have more pronounced charge-transfer character, with the probability at nearest neighbor higher than the probability at the hole site.

In order to address the validity of our calculations, based on the  $Pa\bar{3}$  lattice, with respect to the real, glassy crystal, we repeated the zero-pressure calculations with five different orientations of the molecule. As a result, the electronic gap fluctuated from 2.0 to 2.2 eV. That establishes an uncertainty in the determination of energy gaps arising from orientational disorder of the molecules. We find that orientational disorder affects similarly the electronic and optical gaps. The exciton binding energy fluctuates by less than 0.1 eV upon rotation of the molecular unit. Fine features in the absorption spectrum and in the density of states are smoothed out by molecular disorder while the broader features (energy position and width of major peaks) are very robust.

#### IV. FULLERITE AT HYDROSTATIC PRESSURE

Figure 1 shows that the electronic and optical gaps decrease continuously as an hydrostatic pressure of up to 6 GPa is applied on crystalline  $C_{60}$ . The overall decrease in electronic gap is 0.9 eV with pressure ranging from zero to 6 GPa. To our knowledge, the electronic gap at high hydrostatic pressure has not been measured yet. The optical gap (*i.e.*, the excitation energy of the first bound exciton) decreases by 0.7 eV in the same pressure range. Since that exciton is optically inactive, the best comparison of optical activity as a function of pressure should be done following the position of the first peak in the absorption spectrum, on Figure 3. The peak moves from 2.2 eV to 1.75 eV in the pressure range from zero to 6 GPa. This is compatible with the first determinations of transmission edge as a function of pressure<sup>15</sup>: the transmission edge decreases from 1.9 eV (zero pressure) to 1.5 eV (5 GPa).

Figure 1 also shows that the profile of energy gap versus lattice parameter is not linear. A suitable model for the dependence of the gap with respect to pressure should take into account the behavior of dielectric screening for different amounts of intermolecular spacing and hence different amounts of overlap between molecular orbitals at different molecules. Snoke and collaborators<sup>15</sup> have proposed a phenomenological model for the gap.

Meletov and Dolganov<sup>10</sup> have also found a decrease in the optical gap as a function of pressure. In their experiment, microcrystals of fullerite were placed inside a diamond anvil cell, with pressure of up to 2.5 GPa. Several phenomena were observed in that experiment:

1. At zero pressure, a low-energy line and two well pronounced lines in the absorption spectrum were found, labeled A (at 2.0 eV), B (2.7 eV) and C (3.5 eV) respectively. Line A is very weak and it could originate from transitions  $H_u \rightarrow T_{1u}$ , which gain finite oscillator strength from mixing with higher transitions. That interpretation is supported by our calculations, which indicate an onset of the line at 1.7 eV and very small but non-vanishing oscillator strength.
2. Lines B and C have similar strength. It was found experimentally that optical activity migrates from C to B as the microcrystals are compressed. That effect is found in Figure 3, where we see enhancement of the peak at 2.2 eV and reduction of the peak at 3.5 eV, while both peaks redshift from zero to 3.4 GPa. Since we also see mixing between transitions  $H_u \rightarrow T_{1g}$  and  $H_g \rightarrow T_{1u}$ , the major components of peaks B and C respectively, our calculations confirm the assumption that migration of optical activity is caused by mixing between different optical transitions<sup>10</sup>.
3. The energy dependence of the measured absorption spectrum was reported to be weakly dependent on pressure in the pressure range from zero to 2.5 GPa<sup>10</sup>. Figure 3 confirms that observation. At the next pressure value (6.1 GPa), the two peaks merge into an asymmetric wide peak. That indicates that bands derived from different molecular multiplets start to overlap, as shown in Figure 4.

Hydrostatic pressure also modifies the character of bound excitons, making them more delocalized. Comparing the distribution of probabilities at zero pressure (lattice parameter 14.2 Å) and 3.4 GPa (lattice parameter 13.6 Å), Table I shows that the first bound exciton becomes substantially more delocalized, with a correlation radius between the first and third

nearest-neighbor distances. We believe that two mechanisms contribute to delocalization: applied pressure increases the overlap of molecular orbitals on different molecules, thus increasing the probability of one electron moving from one molecule to its neighbor; and pressure also increases the mixing between bands, particularly between transition  $H_u \rightarrow T_{1u}$  and higher transitions.

As in the zero-pressure regime, we use the  $Pa\bar{3}$  lattice to perform calculations at hydrostatic pressure, with no orientational disorder. Our estimates of the impact of disorder on the energy gap, mentioned at the end of the previous section, also apply to the regime of finite pressure. Since our calculations do not contain accurate van der Waals forces, we have not attempted to investigate the emergence of different glassy phases as a function of pressure. Including accurate van der Waals forces would remove the inaccuracy of the calculated gaps with respect to orientational disorder in fullerite.

## V. FULLERITE WITH INTERCALATED MOLECULES

Fullerene  $C_{60}$  is very stable, which favors the engineering of microcrystals with intercalated molecules. At equilibrium, the FCC crystal has two large types of voids: an octahedral site with radius 3.5 Å and a tetrahedral site with radius 1.15 Å. Isolated atoms and small molecules can be easily placed in one of those voids. Doped  $C_{60}$  has very interesting properties, for instance  $K_3C_{60}$  is superconductor at 18 K<sup>7</sup>.  $Ca_3C_{60}$  is superconductor at 8.4 K<sup>6</sup>. Those compounds also show significant electron transfer from dopant atom to cage. Doping fullerite with wide-gap molecules produce different phenomena. Depending on the concentration and symmetry of the dopant, it can lower the symmetry of the host crystal and enhance the oscillator strength of otherwise dark optical transitions of fullerite. Highly-symmetric dopants are expected to produce less distortions in the host. In particular, cubane ( $C_8H_8$ ) has been proposed as an ideal intercalator<sup>11</sup>. It has perfect cubic symmetry. If placed in an octahedral void, it will preserve the cubic symmetry of the lattice. With doping, the crystal is forced to expand isotropically in order to accommodate the extra molecules but no additional structural distortion is necessary. In addition, solid cubane is bound by weak van der Waals forces<sup>32</sup>, which means that cubane is not likely to segregate into clusters. The ionization potential of molecular cubane is 8.6 eV<sup>33</sup>. Its electron affinity is negative, indicating that it has an energy gap in the ultraviolet range. Since the band edges of  $C_{60}$

are inside the ones of cubane, cubane can be used to mimic negative hydrostatic pressure in fullerite without altering the optical properties of the host<sup>11</sup>.

We built a lattice of cubane-fullerene with maximum doping by filling all octahedral voids in the FCC lattice with cubane. The lattice parameter is taken as 14.8 Å, following experimental determination of the rotor-stator phase<sup>11</sup>. The band structure of this compound around its energy gap is very similar to undoped fullerite with the same lattice constant. Cubane derived bands are found no less than 4 eV away from the gap. The electronic gap of fullerite with intercalated cubane ( $C_8H_8-C_{60}$ ), obtained from our GW calculations is 2.6 eV, similar to the electronic gap obtained for fullerite with the same lattice parameter (2.7 eV). The difference of 0.1 eV is close to the numerical precision of our calculations.  $C_8H_8-C_{60}$  and pristine fullerite also have similar optical gaps: 2.0 eV and 1.85 eV. Figure 5 shows that the absorption spectra of  $C_8H_8-C_{60}$  and pristine fullerite differ from each other only above 3.5 eV. These findings confirm that the effect of adding cubane is, by and large expand the lattice of fullerene molecules. All other phenomena in its electronic structure are direct consequences of lattice expansion.

Other intercalants can also produce lattice expansion. Atoms of noble gases are good candidates, owing to their low reactivity and high energy gap. One shortcoming is that they are smaller than cubane. While these molecules will not expand the lattice significantly, a small change in gap can be measured. Therefore, fullerite could be used as a sensor of inert molecules. Significant expansion could be obtained by overdoping fullerite with several atoms per interstitial site. Other candidates are small molecules such as methane ( $CH_4$ ), hydrogen ( $H_2$ ) or nitrogen ( $N_2$ ).

## VI. SUMMARY AND PERSPECTIVES

The results presented above show that several properties of fullerite, particularly the threshold of its optical absorption, can be tuned by applying pressure. By applying hydrostatic pressure of up to 6 GPa, easily obtained in diamond anvil cell devices, the first peak of optical absorption redshifts from 2.2 eV (yellow-green) to 1.8 eV (red), thus making microcrystals less transparent. Similar reduction in the gap as a function of pressure has been reported in alkali-doped fullerite<sup>12</sup>. Applications of this phenomenon are plenty. One of them is in piezo-optical sensors: one can put clean microcrystals of fullerite in an envi-

ronment under unknown pressure and infer the pressure by measuring their transmittance or absorbance. This is particularly useful if the microcrystals are part of a microdevice, subject to pressure gradients and where usual pressure gauges cannot be used.

One can expand the range of colors where fullerite gauges operate by doping microcrystals with weakly interacting molecules. It has been shown experimentally that saturating microcrystals with cubane increases its lattice parameter<sup>6</sup>. Our results show that the lattice expansion produces a blueshift of the first absorption peak from 2.2 eV to around 2.6 eV. Other dopants can produce larger lattice expansion and hence larger blueshifts, depending on their size and concentration.

In summary, we have done first-principles calculations of electronic and optical properties of fullerite in order to characterize their pressure dependence. Comparison between available experimental data and our calculations at equilibrium lattice parameter show that our methodology predicts gaps with an accuracy of 0.1 to 0.2 eV. The absorption edge shifts toward the red end of the spectrum as we apply hydrostatic pressure of up to 6 GPa. There is little distortion in the electronic structure of the material in the pressure range investigated. We have also confirmed earlier hypotheses that cubane-intercalated fullerite has optical properties very similar to fullerite with an artificial lattice expansion. These findings show that pure fullerite or fullerite with inert dopants can be used as active element in piezo-optical sensors.

We would like to thank discussions with E. Schwegler, T. Ogitsu and H. Whitley for discussions. Research sponsored by the Division of Materials Sciences and Engineering BES, U.S. DOE under contract with UT-Battelle, LLC. Computational support was provided by the National Energy Research Scientific Computing Center.

---

<sup>1</sup> H. Kroto, J. Heath, S. O'Brien, R. Curl, and R. Smalley, *Nature* **318**, 162 (1985).

<sup>2</sup> M. S. Dresselhaus, G. Dresselhaus, and P. C. Eklund, *Science of fullerenes and carbon nanotubes: their properties and applications* (Academic Press, San Diego, 1996).

<sup>3</sup> W. Kratschmer, L. Lamb, K. Fostiropoulos, and D. Huffman, *Nature* **347**, 354 (1990).

<sup>4</sup> X. Blase, P. Gillet, A. San Miguel, and P. Mélinon, *Phys. Rev. Lett.* **92**, 215505 (2004).

<sup>5</sup> A. San Miguel, *Chem. Soc. Rev.* **35**, 876 (2006).

- <sup>6</sup> A. Kortan, N. Kopylov, S. Glarum, E. Gyorgy, A. Ramirez, R. Fleming, F. Thiel, and R. Haddon, *Nature* **355**, 529 (1992).
- <sup>7</sup> A. Hebard, M. Rosseinsky, R. Haddon, D. Murphy, S. Glarum, T. Palstra, A. Ramirez, and A. Kortan, *Nature* **350**, 600 (1991).
- <sup>8</sup> K. Meletov and G. Kourouklis, *J. Exp. Theor. Phys.* **100**, 760 (2005).
- <sup>9</sup> B. Sundqvist, *Adv. Phys.* **48**, 1 (1999).
- <sup>10</sup> K. Meletov and V. Dolganov, *J. Exp. Theor. Phys.* **86**, 177 (1998).
- <sup>11</sup> S. Pekker, E. Kovats, G. Oszlanyi, G. Benyei, G. Klupp, G. Bortel, I. Jalsovszky, E. Jakab, F. Borondics, K. Kamaras, et al., *Nature Mat.* **4**, 764 (2005).
- <sup>12</sup> R. Poloni, M. V. Fernandez-Serra, S. Le Floch, S. De Panfilis, P. Toulemonde, D. Machon, W. Crichton, S. Pascarelli, and A. San-Miguel, *Phys. Rev. B* **77**, 035429 (2008).
- <sup>13</sup> S. Duclos, K. Brister, R. Haddon, A. Kortan, and F. Thiel, *Nature* **351**, 380 (1991).
- <sup>14</sup> M. Núñez Regueiro, L. Marques, J. L. Hodeau, O. Béthoux, and M. Perroux, *Phys. Rev. Lett.* **74**, 278 (1995).
- <sup>15</sup> D. W. Snoke, K. Syassen, and A. Mittelbach, *Phys. Rev. B* **47**, 4146 (1993).
- <sup>16</sup> F. Moshary, N. H. Chen, I. F. Silvera, C. A. Brown, H. C. Dorn, M. S. de Vries, and D. S. Bethune, *Phys. Rev. Lett.* **69**, 466 (1992).
- <sup>17</sup> M. Kozlov and K. Yakushi, *J. Physics - Condens. Matter* **7**, L209 (1995).
- <sup>18</sup> E. L. Shirley and S. G. Louie, *Phys. Rev. Lett.* **71**, 133 (1993).
- <sup>19</sup> E. L. Shirley, L. X. Benedict, and S. G. Louie, *Phys. Rev. B* **54**, 10970 (1996).
- <sup>20</sup> C. Hartmann, M. Zigone, G. Martinez, E. L. Shirley, L. X. Benedict, S. G. Louie, M. S. Fuhrer, and A. Zettl, *Phys. Rev. B* **52**, R5550 (1995).
- <sup>21</sup> R. W. Martin, *Electronic structure: basic theory and practical methods* (Cambridge University Press, Cambridge, UK, 2004).
- <sup>22</sup> J. P. Perdew, K. Burke, and M. Ernzerhof, *Phys. Rev. Lett* **77**, 3865 (1996).
- <sup>23</sup> M. S. Hybertsen and S. G. Louie, *Phys. Rev. B* **34**, 5390 (1986).
- <sup>24</sup> W. Aulbur, L. Jönsson, and J. Wilkins, *Solid State Physics* (Academic Press, New York, 2000), vol. 54, p. 1.
- <sup>25</sup> G. Onida, L. Reining, and A. Rubio, *Rev. Mod. Phys.* **74**, 601 (2002).
- <sup>26</sup> M. Rohlfing and S. G. Louie, *Phys. Rev. B* **62**, 4927 (2000).
- <sup>27</sup> A. L. Fetter and J. D. Walecka, *Quantum Theory of Many-Particle Systems* (Mc-Graw Hill,

New York, 1971).

- <sup>28</sup> M. L. Tiago and J. R. Chelikowsky, Phys. Rev. B **73**, 205334 (2006).
- <sup>29</sup> C. D. Spataru, S. Ismail-Beigi, R. B. Capaz, and S. G. Louie, Phys. Rev. Lett. **95**, 247402 (2005).
- <sup>30</sup> M. L. Tiago, P. R. C. Kent, R. Q. Hood, and F. A. Reboredo, J. Chem. Phys. **129**, 084311 (2008).
- <sup>31</sup> F. A. Cotton, *Chemical Applications of Group Theory* (J. Wiley and Sons, New York, 1990).
- <sup>32</sup> T. Yildirim, P. M. Gehring, D. A. Neumann, P. E. Eaton, and T. Emrick, Phys. Rev. Lett. **78**, 4938 (1997).
- <sup>33</sup> C. Lifshitz and P. Eaton, Int. J. Mass Spectrom. Ion Phys. **49**, 337 (1983).

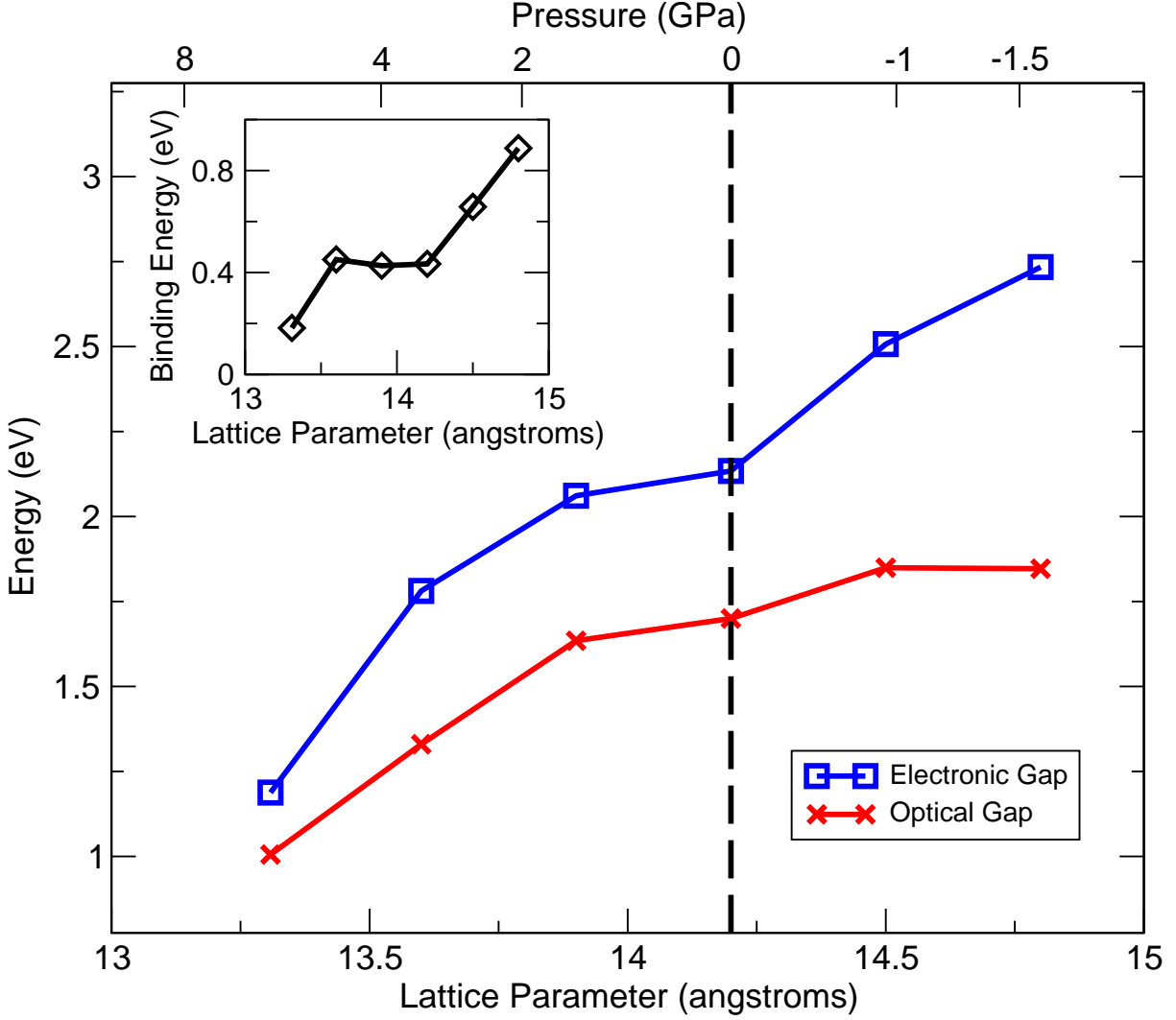


FIG. 1: (Color online) Electronic gap (squares) and optical gap (crosses) calculated for fullerite as functions of lattice parameter. The equivalent hydrostatic pressure was obtained using Vinet equation, Equation 4. The electronic gap was calculated within the GW approximation. The optical gap shown is the energy of the first excitation energy obtained from the BSE. It is a lower bound to the experimental optical gap since the first excitation has very low oscillator strength (see text). The inset shows the maximum exciton binding energy, *i.e.* difference between the electronic and optical gaps.

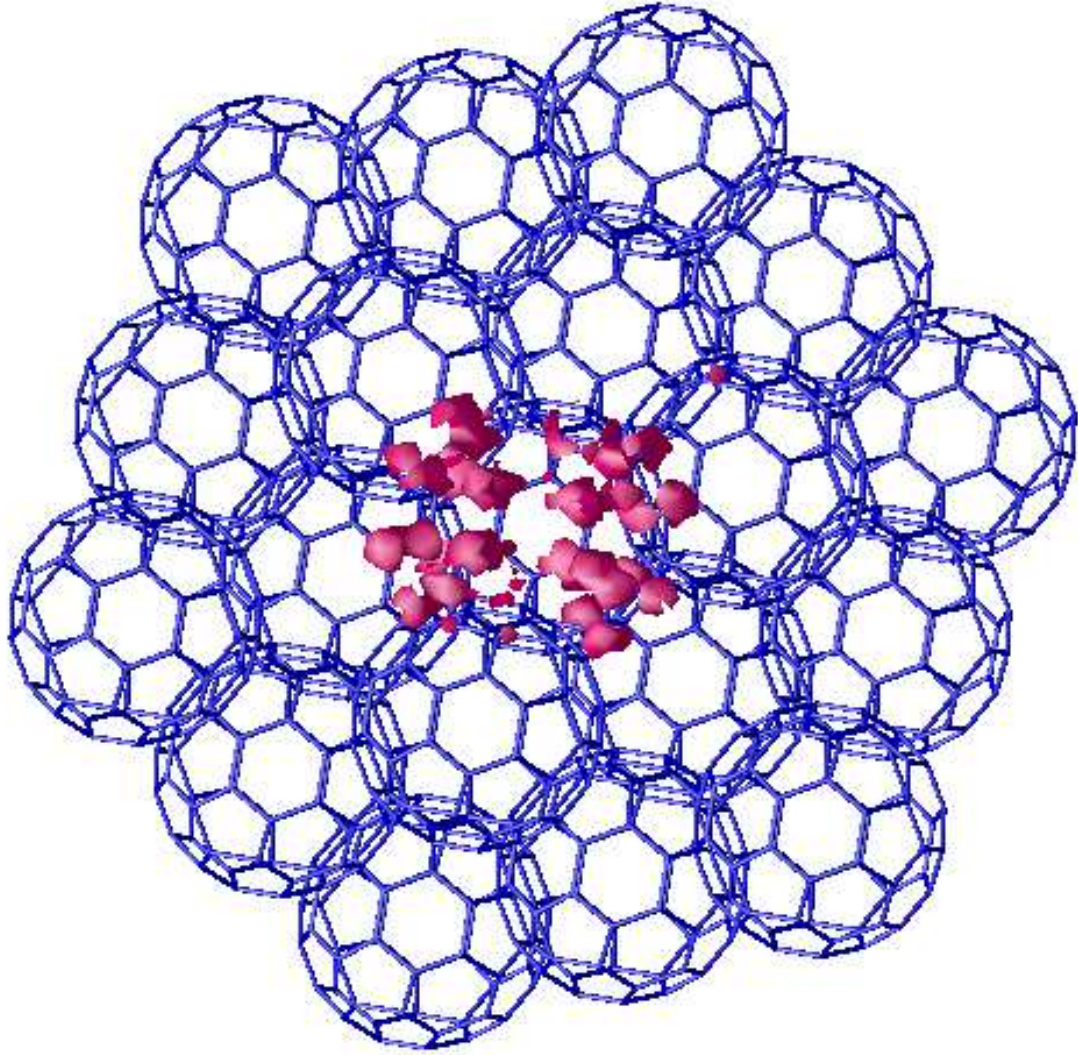


FIG. 2: (Color online) Isocontour plot of the electron probability distribution function of the first bound exciton provided that the hole is at a position where the highest occupied molecular orbital has maximum amplitude. The plot corresponds to fullerite at zero pressure. Only molecules up to second neighbor from the hole site are depicted in the figure. The isocontour shown corresponds to a value 10% lower than the maximum value of the probability distribution. This exciton is composed primarily by transitions in the  $H_u \rightarrow T_{1u}$  multiplet.

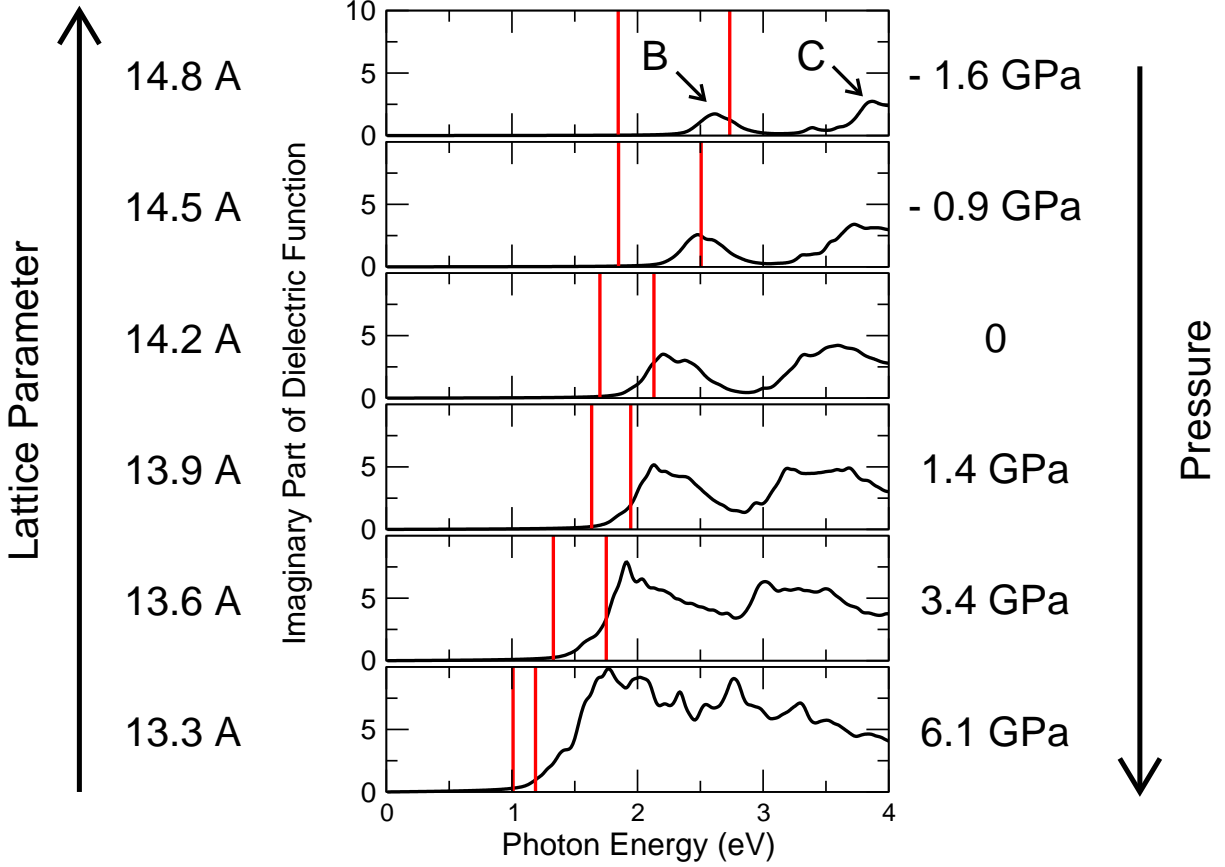


FIG. 3: (Color online) Imaginary part of the dielectric function for several choices of lattice parameter. Vertical bars on each panel indicate the calculated optical and electronic gaps. An artificial Gaussian broadening of 0.02 eV was added to all absorption spectra. Sharp features in the spectrum are expected to fade away with inclusion of rotational disorder. Line A in the measured spectrum<sup>10</sup> (see text) is very weak to be visible. Line B is the first absorption line, at around 2.2 eV at zero pressure. Line C is the second absorption line, at around 3.6 eV at zero pressure.

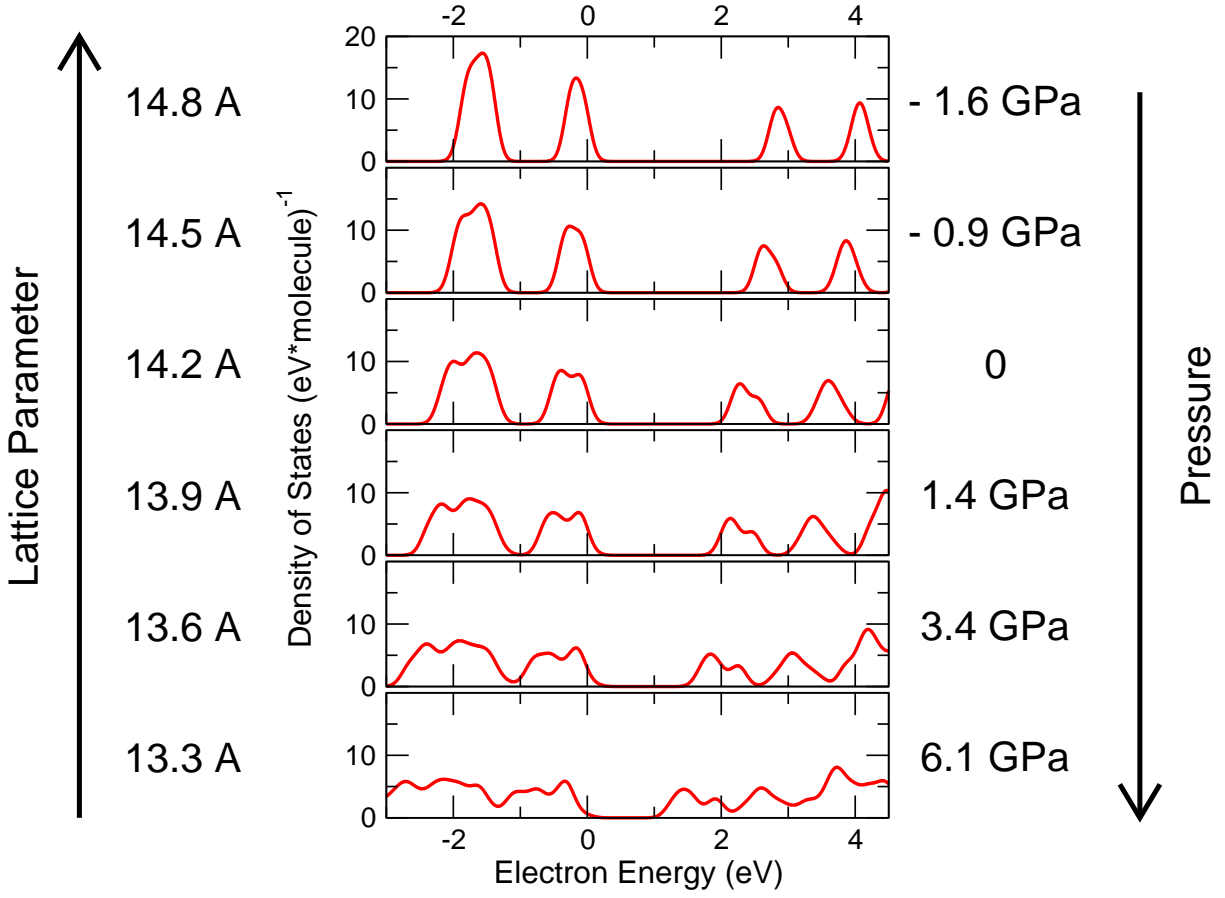


FIG. 4: (Color online) Density of states in fullerite for several choices of lattice parameter, obtained within the GW theory. Energies are defined with respect to the valence band maximum. A Gaussian broadening of 0.1 eV was added to all density distributions. The five major features in the density of states (well separated at zero and “negative” pressure) correspond to different molecular multiplets, from lower to higher energy:  $H_g+G_g$  (superimposed),  $H_u$ ,  $T_{1u}$ ,  $T_{1g}$ .

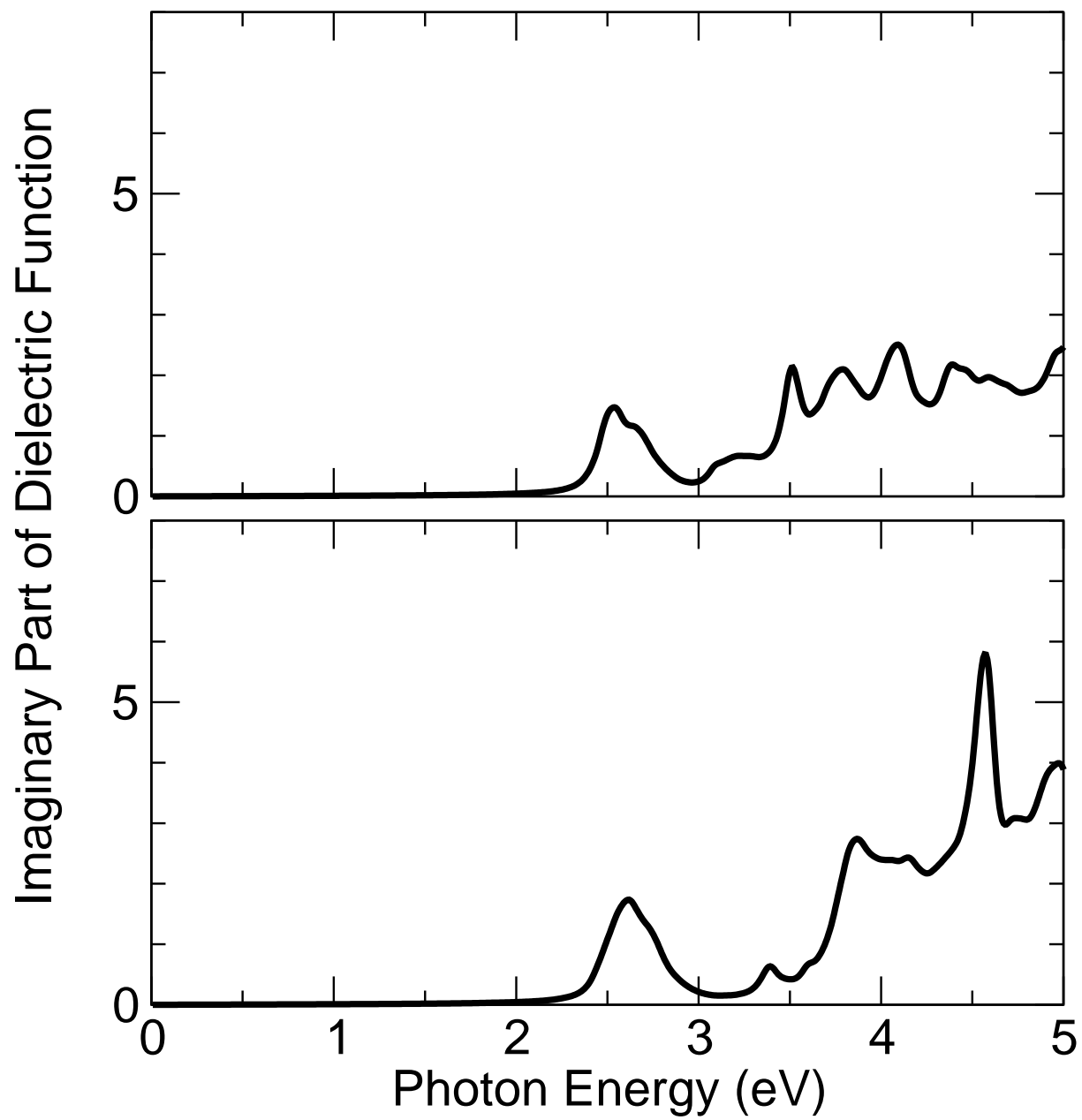


FIG. 5: Imaginary part of the dielectric function of  $C_8H_8-C_{60}$  (a) and pure  $C_{60}$  (b). An artificial Gaussian broadening of 0.02 eV was added to all absorption spectra.

Location of Electron	Probability		
	$a = 13.6\text{\AA}$	$a = 14.2\text{\AA}$	$a = 14.8\text{\AA}$
Hole's molecule	15 %	62 %	84 %
1 <sup>st</sup> Nearest Neighbor	25 %	30 %	13 %
2 <sup>nd</sup> Nearest Neighbor	10 %	2 %	< 1%
3 <sup>rd</sup> Nearest Neighbor	25 %	3 %	< 1 %

TABLE I: Electron probability distribution of the first bound exciton calculated as a function of the distance to the hole. The probability was integrated over each shell of molecules around the molecule that contains the hole. The integration was performed over a Wigner-Seitz cell centered on each molecule. Three different lattice parameters are shown: 13.6 Å (3.4 GPa), 14.2 Å (zero pressure) and 14.8 Å (negative pressure -1.6 GPa).